

Jet-veto in bottom-quark induced Higgs production at next-to-next-to-leading order

Robert V. Harlander and Marius Wieseemann

Fachbereich C, Bergische Universität Wuppertal

42097 Wuppertal, Germany

harlander@physik.uni-wuppertal.de

m.wieseemann@uni-wuppertal.de

Abstract

We present results for associated Higgs+ n -jet production in bottom quark annihilation, for $n = 0$ and $n \geq 1$ at NNLO and NLO accuracy, respectively. We consider both the cases with and without b -tagging. Numerical results are presented for parameters relevant for experiments at the LHC.

1 Introduction

The Standard Model (SM) and its supersymmetric extensions require a mechanism to explain the gauge boson and fermion masses. The Higgs mechanism where the particles acquire masses through interactions with the Higgs field(s) is the most popular ansatz. One of the primary goals of the Large Hadron Collider (LHC) is to find or exclude a Higgs boson over the full theoretically meaningful mass range.

Various channels can be exploited for the search of Higgs bosons at hadron colliders (see, e.g., Refs. [1, 2]). While in the SM gluon fusion has the largest cross section by far, in supersymmetric (SUSY) theories the radiation off bottom-quarks becomes equally important (see, e.g., Ref. [3]):

$$pp \rightarrow (b\bar{b})H + X. \quad (1)$$

Here and in what follows, H denotes a generic neutral Higgs boson, scalar or pseudo-scalar. In particular, it includes the light and heavy CP-even as well as the CP-odd neutral Higgs bosons of the Minimal Supersymmetric Standard Model (MSSM), h^0 , H^0 , and A .

Two approaches have been pursued in the literature to calculate the process (1). In the so-called “four-flavor scheme” (4FS), the leading order (LO) processes are

$$gg/q\bar{q} \rightarrow b\bar{b}H, \quad (2)$$



Figure 1: Leading order diagrams for the associated production of a Higgs with bottom-quarks in the (a) four- and (b) five-flavor scheme.

where $q \in \{u, d, s, c\}$. The collinear region of the bottom-quark momenta occurring in the gg initiated process, see Fig. 1(a), is regulated by the bottom-quark mass m_b and leads to potentially large logarithms $\ln(\mu_F^2/m_b^2)$, where $\mu_F \simeq m_H$ denotes the factorization scale, and m_H the Higgs mass. In this approach, the total cross section for a scalar Higgs boson is known to next-to-leading order (NLO) QCD accuracy [4, 5]; SUSY effects have been considered as well [6].

The other approach to calculate the cross section for the process in Eq. (1) is the so-called “five-flavor scheme” (5FS), where the LO partonic reaction is

$$b\bar{b} \rightarrow H. \quad (3)$$

The corresponding Feynman diagram is shown in Fig. 1(b). The DGLAP evolution of the bottom-quark parton densities formally resums the collinear logarithms that are manifest in the 4FS, see above, leading to a better perturbative convergence. However, effects from bottom-quark production at large transverse momentum p_T are taken into account only at higher orders in the 5FS. In fact, the next-to-next-to-leading order (NNLO) prediction [7] plays a special role in this process because only from this order on, the 5FS approach includes the LO diagram of the 4FS (see Ref. [7] for a more detailed discussion). In the 5FS, also electro-weak corrections have been evaluated [8].

Both the 4FS and 5FS are formally viable approaches to calculate the inclusive cross section for the process shown in Eq. (1). Nevertheless, it took a significant amount of efforts to pin down their qualitative and quantitative differences (see, e.g., Refs. [7, 9–11]). The “LHC Higgs Cross Section Working Group” [12] has now decided to combine the inclusive cross sections of both schemes according to the so-called “Santander Matching” procedure [13]. In order to optimally exploit the advantages of each approach in its region of applicability, they enter the cross section prediction with a Higgs-mass dependent weight in this procedure.

In summary, the inclusive Higgs cross section in bottom-quark annihilation is under good theoretical control. However, it is well known that exclusive H +jet production can be advantageous for experimental analyses. In gluon fusion, this process has been studied in quite some detail, both in the SM [14–26] and the Minimal Supersymmetric Standard



Figure 2: Representative diagrams of the leading order channels (a) $b\bar{b} \rightarrow gH$ and (b) $bg \rightarrow bH$.

Model (MSSM) [27–32]. As mentioned above, in the MSSM it is essential to take $(b\bar{b})H$ +jet production into account as well. In this paper we present the corresponding cross sections in the framework of the 5FS. In particular, we show results for the Higgs plus 0- and ≥ 1 -jet cross sections for Higgs production in bottom-quark annihilation at NNLO and NLO, respectively. The results are given in the SM, but according to the studies of Refs. [8, 33], they are applicable to the MSSM by simply rescaling the $b\bar{b}H$ coupling.

Let us stress at this point the difference between this study and similar ones existing in the literature. In Ref. [34], we calculated kinematical distributions of the Higgs boson in H +jet production, while here we focus on the aspect specific to the associated jets. Ref. [35] considered the NLO cross section for Higgs production in association with one or two *bottom* jets ($H + nb$ -jets, $n = 1, 2$), which is contained in our calculation and which we used as an important check. The analogous study in the 4FS has been performed in Ref. [36]. Our viewpoint here is simply that bottom-induced Higgs production may actually be the dominant mechanism for Higgs production, so that the studies done for H +jet production in gluon fusion should be supplemented by the bottom-annihilation contribution. Nevertheless, we will also include updated numbers for $H + nb$ -jet production ($n = 1, 2$) in this paper, and present NNLO results for a b -jet veto, i.e. for $H + 0b$ -jet production. One caveat should be added, however, namely that for a fully consistent combination of gluon fusion and $b\bar{b}H$ production, one would have to include interference terms of these two processes which will be neglected in what follows (as it has been done in all existing studies of the inclusive cross section up to now).

The remainder of this paper is organized as follows: In Section 2, we describe our calculation of the $H + n$ -jet ($n = 0$ and $n \geq 1$) and the $H + nb$ -jet cross section ($n = 0, 1, 2$). Section 3 contains our results for a default set of parameters. In particular, we consider proton-proton collisions at 7 TeV, while the numbers for 14 TeV center-of-mass energy are collected to Appendix B. Our conclusions are presented in Section 4.

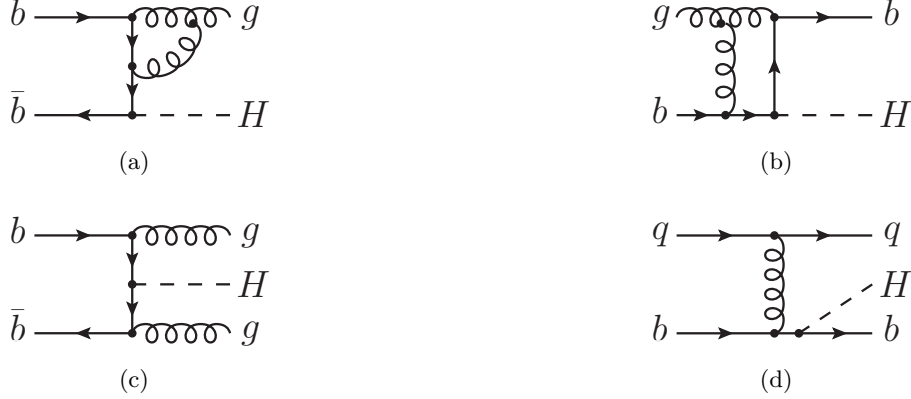


Figure 3: Representative diagrams at NLO: (a),(b) virtual and (c),(d) real corrections.

2 Calculation of $(b\bar{b})H$ +jet production

Considering H +jet production in bottom-quark annihilation at NLO, several subprocesses have to be taken into account. The generic leading order channels are $b\bar{b} \rightarrow gH$ and $gb \rightarrow bH$, see Fig.2. In Fig.3(a) and 3(b), two representative diagrams of the corresponding virtual corrections to $b\bar{b} \rightarrow gH$ and $gb \rightarrow bH$ are shown. The real emission processes derived from the LO channels are $b\bar{b} \rightarrow ggH$, $b\bar{b} \rightarrow b\bar{b}H$, $b\bar{b} \rightarrow q\bar{q}H$, and $gb \rightarrow bgH$. In addition, the sub-channels $gg \rightarrow b\bar{b}H$, $qb \rightarrow qbH$, $bb \rightarrow bbH$, and $q\bar{q} \rightarrow b\bar{b}$ ($q \in \{u, d, s, c\}$) which do not have a LO correspondence need to be taken into account. Two representative real emission diagrams are displayed in Fig.3(c) and 3(d). It is understood that the charge conjugated processes must be included as well. We note that diagrams where the Higgs boson is radiated off of closed top or bottom quark loops are usually attributed to the gluon fusion channel, and therefore are not taken into account here. As already pointed out in the introduction, for a consistent treatment of the $H + n$ -jet cross section these two processes should be combined, and also interference terms should be taken into account.

The calculation was carried out using the program described in Ref. [34], where we implemented the anti- k_T jet-algorithm¹ [37] to identify QCD jets.

2.1 Cross section without jet-flavor tagging

Our setup allows us to calculate the exclusive and inclusive $H + n$ -jet cross sections $\sigma_{n\text{-jet}}$ and $\sigma_{\geq n\text{-jet}}$, respectively, where for $n = 1$ we work at NLO accuracy, while for $n = 2$ we only get a LO result. (The inclusive and exclusive $H + 2$ -jet cross section are identical at

¹Since at most two jets can occur at the order we are considering, the anti- k_T leads to the same results as the k_T and the Cambridge-Aachen algorithm.

this order, $\sigma_{\geq 2\text{-jet}} = \sigma_{2\text{-jet}} + \mathcal{O}(\alpha_s^3)$, where α_s is the strong coupling constant.) Since our results do not include any parton showering or hadronization, “jet” denotes any outgoing quark, anti-quark or gluon, irrespective of the quark flavor. Further below, we will also consider the case of b -tagged cross sections.

With the knowledge of the total inclusive cross section σ_{tot} up to NNLO [7] we can use our program for the inclusive $H + 1\text{-jet}$ rate (also referred to as $H + \geq 1\text{-jet}$ or inclusive $H + \text{jet}$ rate in the following) at NLO to obtain the exclusive $H + 0\text{-jet}$, or jet-vetoed, cross section at NNLO:

$$\sigma_{\text{jet-veto}}^{\text{NNLO}} \equiv \sigma_{0\text{-jet}}^{\text{NNLO}} = \sigma_{\text{tot}}^{\text{NNLO}} - \sigma_{\geq 1\text{-jet}}^{\text{NLO}'} . \quad (4)$$

Since this quantity is formally of NNLO, both contributions on the right side of Eq. (4) have to be calculated with NNLO parton density functions (PDFs) and couplings. This is indicated by the prime in $\sigma_{\geq 1\text{-jet}}^{\text{NLO}'}$ which distinguishes it from the proper NLO quantity $\sigma_{\geq 1\text{-jet}}^{\text{NLO}}$. Similar to the fact that $\sigma_{1\text{-jet}}^{\text{NLO}} + \sigma_{2\text{-jet}}^{\text{LO}} \neq \sigma_{\geq 1\text{-jet}}^{\text{NLO}} (\equiv \sigma_{1\text{-jet}}^{\text{NLO}} + \sigma_{2\text{-jet}}^{\text{LO}'})$ due to the different orders of PDFs and couplings that need to be used, it is clear that

$$\sigma_{0\text{-jet}}^{\text{NNLO}} + \sigma_{\geq 1\text{-jet}}^{\text{NLO}} \neq \sigma_{\text{tot}}^{\text{NNLO}} \neq \sigma_{0\text{-jet}}^{\text{NNLO}} + \sigma_{1\text{-jet}}^{\text{NLO}} + \sigma_{2\text{-jet}}^{\text{LO}} . \quad (5)$$

Numerical results for $\sigma_{n\text{-jet}}$ with $n = 0$ and $n \geq 1$ will be presented in Section 3.

2.2 Cross section with tagged b -quarks

If realized in Nature, the bottom-quark annihilation process provides a promising opportunity to measure the bottom-quark Yukawa coupling to the Higgs boson. To this aim, it is useful to define a proper measurement function in order to filter events with a specific number of final state bottom-jets. As already mentioned, the resulting cross section with one and two b -quarks in the final state has been calculated before through NLO and LO, respectively, in Ref. [35]. The calculation is implemented in **MCFM** [38] which we used in order to verify our results within our numerical accuracy of $\lesssim 1\%$.

Due to the finite efficiency ϵ_b of identifying b -jets in the final state, one needs to distinguish the cross section σ_{nb} ($n = 0, 1, 2, \dots$), which is a measure for the number of events with n b -jets in the final state, from the cross section $\sigma_{nb\text{-tag}}$, which concerns the events with n *tagged* b -jets. We require that if the tagging efficiency is 100%, both should be the same:

$$\sigma_{nb\text{-tag}}(\epsilon_b \rightarrow 1) = \sigma_{nb} . \quad (6)$$

Therefore, the *inclusive* $H + b\text{-tag}$ cross section at NLO should be evaluated using [35]

$$\sigma_{\geq 1b\text{-tag}}^{\text{NLO}} = \epsilon_b \sigma_{1b}^{\text{NLO}} + \epsilon_b (2 - \epsilon_b) \sigma_{2b}^{\text{LO}'} , \quad (7)$$

where $\sigma_{2b}^{\text{LO}'}$ is the exclusive $H + 2b$ cross section at LO, evaluated with NLO PDFs and α_s . For the *exclusive*² 1- and 2- b -tagged cross sections, one may use

$$\begin{aligned}\sigma_{1b\text{-tag}}^{\text{NLO}} &= \epsilon_b \sigma_{1b}^{\text{NLO}} + 2\epsilon_b(1 - \epsilon_b)\sigma_{2b}^{\text{LO}}, \\ \sigma_{2b\text{-tag}}^{\text{LO}} &= \epsilon_b^2 \sigma_{2b}^{\text{LO}},\end{aligned}\tag{8}$$

where, in contrast to Ref. [35], we evaluate σ_{2b}^{LO} consistently with LO PDFs and α_s .

The $H + 0b$ -tag cross section can be calculated at NNLO using

$$\sigma_{0b\text{-tag}}^{\text{NNLO}} = \sigma_{0b}^{\text{NNLO}} + (1 - \epsilon_b)\sigma_{1b}^{\text{NLO}} + (1 - \epsilon_b)^2\sigma_{2b}^{\text{LO}}.\tag{9}$$

The first term on the right-hand side refers to events without final state bottom-quarks, the second and third one concerns events with one and two final state bottom-quarks, respectively, none of which is tagged. σ_{1b}^{NLO} and σ_{2b}^{LO} can be calculated directly with the help of our Monte Carlo program, while the $0b$ -contribution is again obtained by subtracting the inclusive cross section for $H + b$ production, evaluated with NNLO PDFs and couplings, from the total rate:

$$\sigma_{0b}^{\text{NNLO}} = \sigma_{\text{tot}}^{\text{NNLO}} - \sigma_{\geq 1b}^{\text{NLO}'}.\tag{10}$$

Numerical results for the individual components of Eqs. (8), (9), and (10) will be presented in Section 3.4.

3 Results

3.1 Preliminary remarks

Before presenting numerical results, let us outline our default parameters. Our choice for the central factorization- and renormalization-scale μ_F and μ_R is $\mu_0 \equiv m_H/4$. Furthermore, all numbers are produced with the MSTW2008 [39] PDFs which implies that the numerical value for the strong coupling constant is taken as $\alpha_s(M_Z) = 0.13939$ at LO, $\alpha_s(M_Z) = 0.12018$ at NLO, and $\alpha_s(M_Z) = 0.11707$ at NNLO. The bottom-Higgs Yukawa coupling is proportional to the bottom-quark mass which we insert in the $\overline{\text{MS}}$ -scheme at the scale μ_R , derived from the input value $m_b(m_b) = 4.2 \text{ GeV}$. No cuts on the Higgs momentum are applied, and jets are defined using the anti- k_T algorithm with jet radius: $R = 0.4$. A jet is required to have transverse momentum of $p_T^{\text{jet}} > 20 \text{ GeV}$ and rapidity $|y^{\text{jet}}| < 4.8$, unless stated otherwise.

All numbers are evaluated for a SM Higgs boson. An MSSM prediction can be obtained by a proper rescaling of the bottom-quark Yukawa coupling. This is true for the two

²In the context of cross sections with b -tags, “exclusive” only refers to the number of final state b -jets; the number of jets without b -quarks is irrelevant.

CP-even, and, due to chiral invariance,³ also for CP-odd Higgs boson (h^0 , H^0 , and A). In this section, we present results for the LHC at 7 TeV. The corresponding numbers for 14 TeV center-of-mass energy can be found in Appendix B.

The theoretical uncertainties of the results presented in this paper have different sources. One of them arises from the PDFs and the input value of $\alpha_s(M_Z)$; we evaluate the corresponding uncertainty according to the method described in Ref. [39], using the 68%CL PDFs. Another source of uncertainty is the truncation of the perturbative series at a fixed order. It is usually estimated from the dependence of the cross section on the unphysical scales μ_F and μ_R . In this paper, we successively fix one of μ_F and μ_R to μ_0 and vary the other within $[0.5\mu_0, 2\mu_0]$; the extreme values of the cross section are then taken as a measure of the perturbative uncertainty. Another uncertainty is induced by the Monte-Carlo integration; it is small, however, and will be neglected throughout this paper.

The perturbative uncertainty of the $H + 0$ -jet cross section has been the subject of some discussion recently. We will come back to this in Section 3.2.

3.2 $H + n$ -jet cross sections without jet-flavor tagging

The first results we present here concern the inclusive H +jet and the exclusive $H + 0$ -jet (or jet-vetoed) cross sections from bottom-quark annihilation through NLO and NNLO, respectively, where no flavor-requirement on the outgoing jets is applied.

Fig. 4 shows the scale variation of the inclusive H +jet rate for a representative Higgs mass of $m_H = 150$ GeV. One observes a significant reduction of the scale dependence when going from LO to NLO, both in μ_F and μ_R , and an excellent consistency between the LO and the NLO predictions when uncertainties are taken into account. This justifies our central scale choice of $\mu_0 = m_H/4$.

Concerning the scale variation of the $H + 0$ -jet cross section, for the gluon fusion process it has been found to be typically of the same order of magnitude or even smaller than for the inclusive cross section [40, 41]. It seems unreasonable then to adopt this variation as the perturbative uncertainty, because the less inclusive character of this observable is expected to introduce an additional effect from the truncation of the perturbative series.

However, we do not observe this behavior for bottom-quark annihilation. For illustration, we consider a Higgs mass of $m_H = 150$ GeV and compare the scale dependence of the $H + 0$ -jet to the total cross section in Fig. 5. The leading order curves are identical, since there are no jets at the partonic level in this case. At higher orders, the $H + 0$ -jet cross section is smaller than the total cross section due to the missing jet contributions, of course. However, the scale dependence reduces when going to higher orders both for the $H + 0$ -jet and the total cross section. While the curves at the various orders for the total cross section are fairly close to each other in the relevant μ -range, they move further apart

³In the 5FS, the bottom quark mass is set to zero.

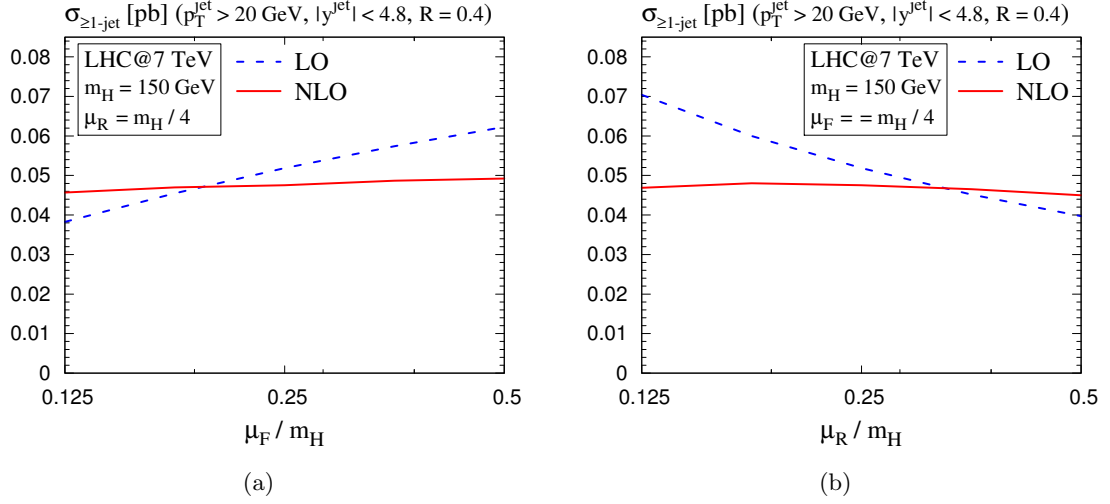


Figure 4: Scale dependence of the inclusive H +jet cross section: (a) μ_F - and (b) μ_R -variation.

for the 0-jet bin for the reasons just discussed. The NNLO curves of the $H + 0$ -jet and the total cross section have an almost identical behavior and are just vertically shifted. The central values differ by roughly a factor of two and, as opposed to gluon fusion [40, 41], the relative uncertainty due to scale variation of the $H + 0$ -jet bin around μ_0 is more than twice as large as for the total cross section.

For gluon fusion it has been suggested to evaluate the perturbative uncertainty of the $H + 0$ -jet cross section from those of its ingredients, i.e. the total and the (primed) inclusive H +jet cross section, see Eq. (4) [41]. Although we just argued that for H production in $b\bar{b}$ -annihilation it is not necessary to adopt this procedure, we provide the corresponding numbers below for completeness.

Fig. 6 shows the decomposition of the total cross section (solid, red; no uncertainties included) into the exclusive $H + 0$ -jet (black, dotted) and the inclusive H +jet (blue, dashed) rates. For illustration, we show the results for both our default jet-rapidity cut of $|y^{\text{jet}}| < 4.8$ as well as for $|y^{\text{jet}}| < 2.5$. One observes that the relative contribution of the inclusive H +jet rate increases with the Higgs mass, similar to what was found for the gluon fusion process [18]. The error bands include the quadratical combination of the perturbative and the PDF+ α_s uncertainties.

The numerical values corresponding to these plots are given in Appendix A in Table 1 and 2 (central values and uncertainties; note Eq. (5)). For completeness, we give in Table 3 also the central values and the perturbative uncertainties of the total inclusive cross sec-

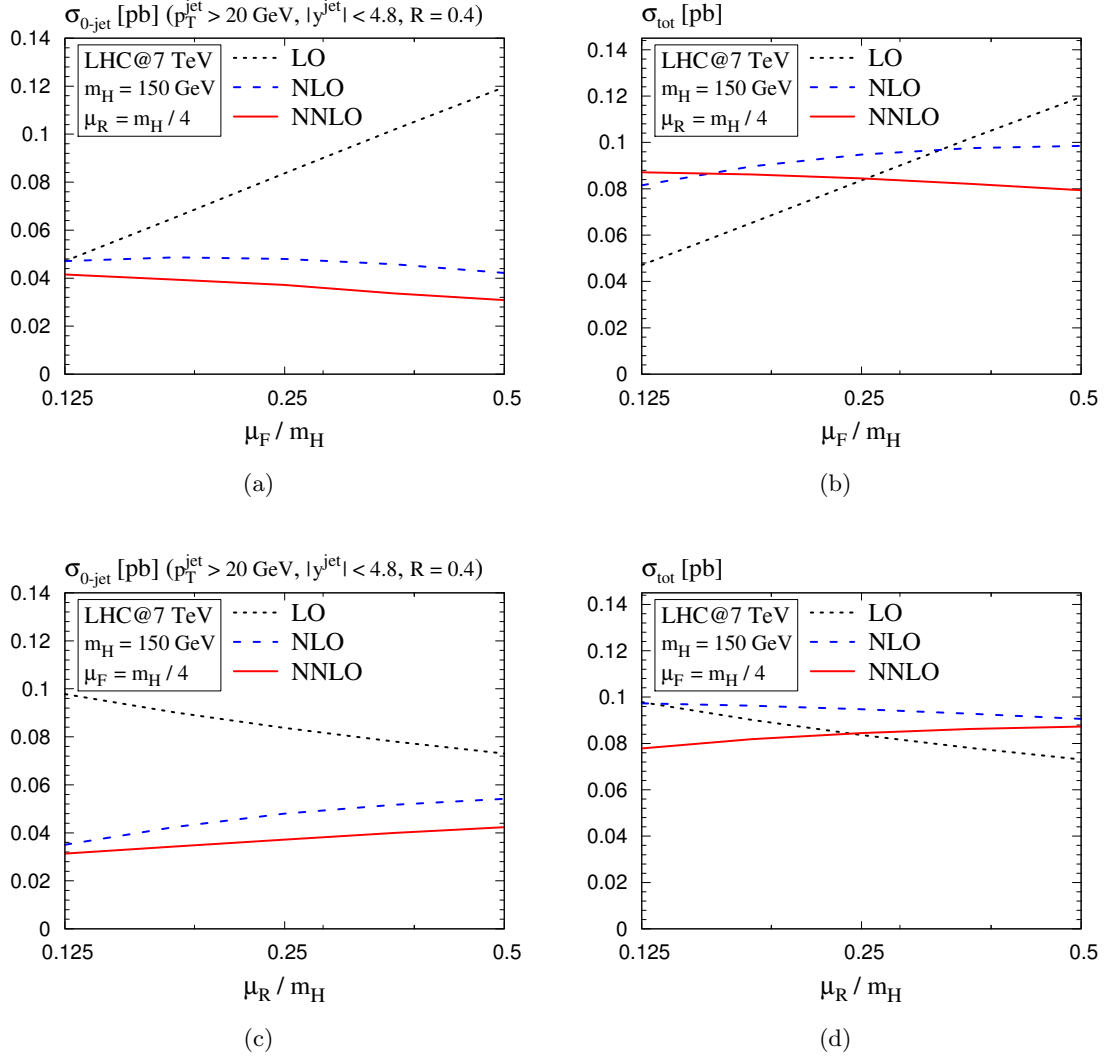


Figure 5: μ_F -dependence of (a) the $H + 0$ -jet cross section and (b) the total cross section, and the μ_R -variation of the same quantities in (c) and (d).

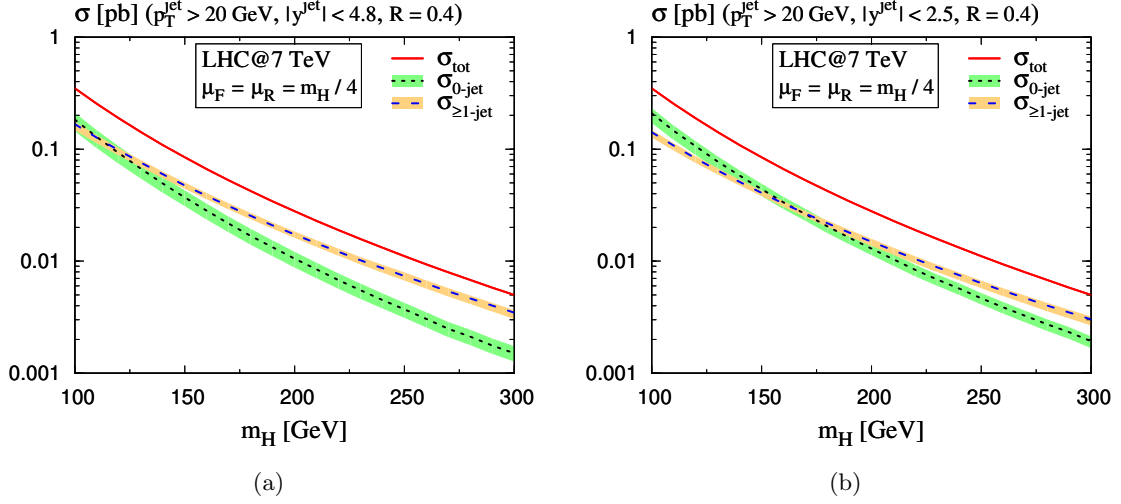


Figure 6: Higgs mass dependence of the $H + 0$ - and ≥ 1 -jet contributions to the total cross section at NNLO and NLO, respectively, for (a) $|y^{\text{jet}}| < 4.8$ and (b) $|y^{\text{jet}}| < 2.5$.

tion at NNLO and the primed inclusive H +jet cross section. This provides all numbers required to calculate the scale uncertainty of the $H + 0$ -jet cross section from those of its ingredients [41].

3.3 Jet distributions

Other potentially useful quantities for Higgs studies at the LHC are the transverse momentum of the hardest jet, $p_{T,1}^{\text{jet}}$, and its rapidity y_1^{jet} . In Fig. 7 we show the $p_{T,1}^{\text{jet}}$ distribution for $|y^{\text{jet}}| < 4.8$ of the inclusive H +jet cross section and the corresponding K -factor. We cut the transverse momentum distribution of the hardest jet at $p_{T,1}^{\text{jet}} = 20$ GeV, below which resummation is required to obtain a reliable result. The scale choice

$$\mu_F = \mu_R = \frac{1}{4} \sqrt{m_H^2 + (p_{T,1}^{\text{jet}})^2} \quad (11)$$

accounts for possible effects that come from jets with high transverse momentum. One observes perturbative corrections of typically less than 10%, and a very weak dependence of the K -factor on $p_{T,1}^{\text{jet}}$ once it is larger than about 50 GeV.

Fig. 8 shows the rapidity distribution of the hardest jet. Contrary to the rapidity distribution of the Higgs (see Ref. [34]), the NLO corrections affect the hardest jet quite significantly, with the K -factor ranging from 0.8 at central jet production to about $K = 2$ in the forward- and backward-region.

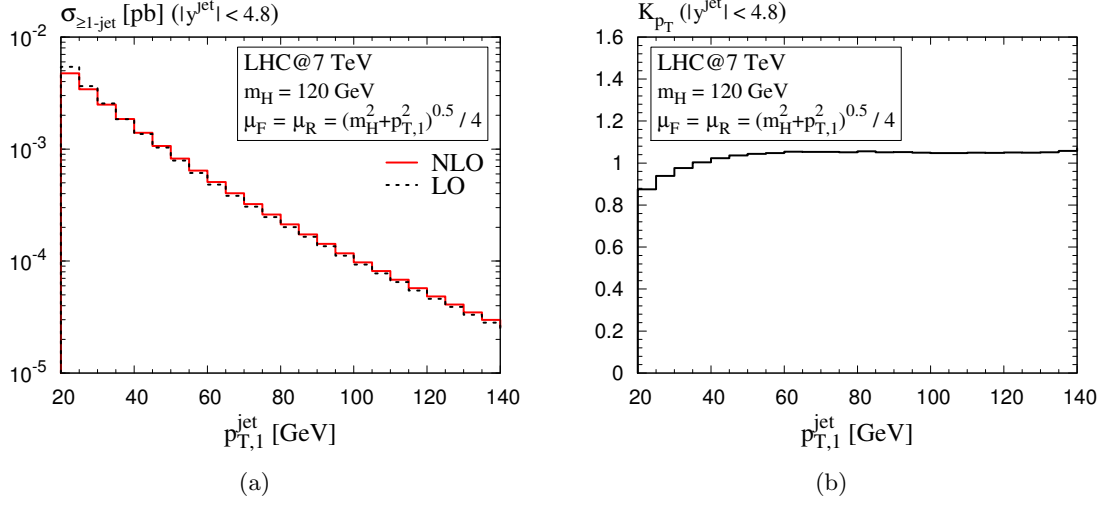


Figure 7: (a) Transverse momentum distribution of the hardest jet in inclusive H +jet production, and (b) the corresponding K-factor.

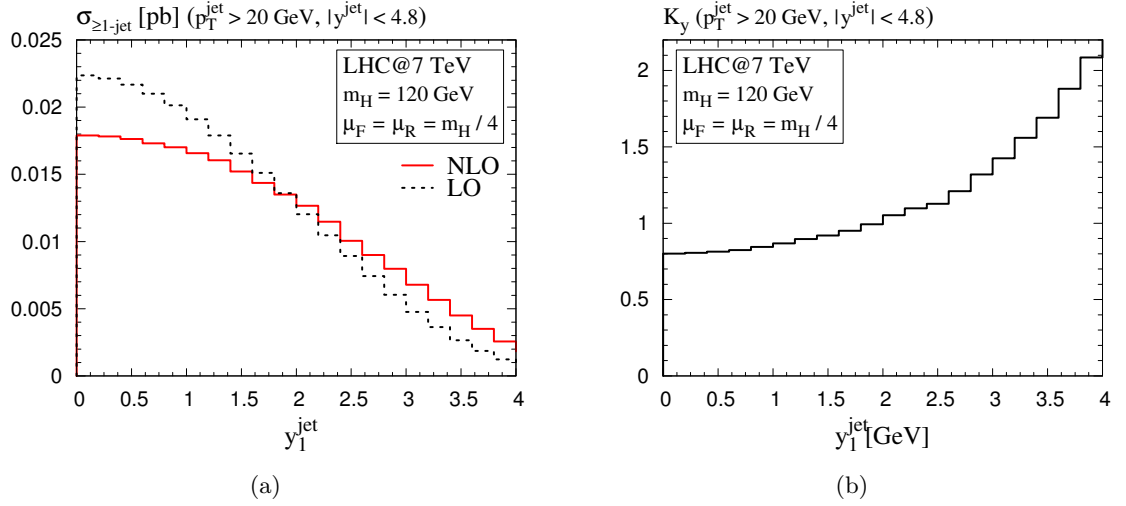


Figure 8: (a) Rapidity distribution of the hardest jet in inclusive H +jet production and (b) the corresponding K-factor.

3.4 $H + nb$ -jet cross section

In this section, we present numerical results for the $H + nb$ -jet cross sections ($n = 0, 1, 2$) as described in Section 2.2. Our default b -jet parameters will be chosen according to the corresponding CMS analysis: $R = 0.5$, $p_T^b > 20$ GeV and $|y^b| < 2.4$. Results for other parameters are available from the authors upon request.

Neglecting the bottom-quark mass, as it is required in the 5FS, leads to divergences in the $H + 1b$ -jet rate which are not cancelled in the sum of all diagrams and counter terms. They arise in the subprocess $b\bar{b} \rightarrow b\bar{b}H$, when a gluon splits into a collinear $b\bar{b}$ pair. In Ref. [35], these divergences were circumvented by introducing an additional cut on the invariant mass of the b -quark pair. We checked that with this cut, these terms contribute less than 1% to the $H + 1b$ -jet rate, which is why we neglect them here. The divergence does not occur in the $H + 2b$ -jet rate, so all contributions can safely be included in this case.

Fig. 9 shows the scale variation of the exclusive $H + 1b$ -jet cross section at LO and NLO and the $H + 2b$ -jet cross section at LO. Similar to the $H + n$ -jet cross sections, one observes a significant reduction of scale dependence for σ_{1b} , when going from LO to NLO. The $H + 2b$ -jet cross section as a LO quantity has a larger scale uncertainty which is obviously dominated by the renormalization scale dependence (see Fig. 9 (c),(d)).

Fig. 10 shows the exclusive $H + 0b$ -jet cross section at LO, NLO and NNLO as a function of the renormalization/factorization scale as evaluated in Eq. (10). We refer to the discussion of $\sigma_{0\text{-jet}}$ in Section 3.2, since its qualitative arguments remain valid for the $H + 0b$ -jet cross section.

Fig. 11 shows the $H + 0b$ -, $1b$ -, and $2b$ -cross sections $\sigma_{0b}^{\text{NNLO}}$, σ_{1b}^{NLO} , and σ_{2b}^{LO} , respectively, as they enter the b -tagged cross sections according to Eqs. (8) and (9). The corresponding numbers are given in Table 4. Similar to the $H + n$ -jet cross sections the relative contributions including b -jets increase for higher Higgs masses.

4 Conclusions

The individual contributions of $H + n$ -jet events for $n = 0$ (jet-veto) and $n \geq 1$ to the total inclusive cross section for Higgs production in bottom-quark annihilation have been presented to NNLO and NLO accuracy. We find a significant reduction of the renormalization- and factorization scale dependence when going to higher perturbative orders. In addition, we have studied kinematical distributions for the hardest emitted jet.

We have also presented an analysis of the $H + nb$ -jet rates for $n = 0, 1, 2$, valid through NNLO, NLO, and LO QCD accuracy, respectively, and observed a similarly good perturbative convergence as for the flavor-unspecific jet result.

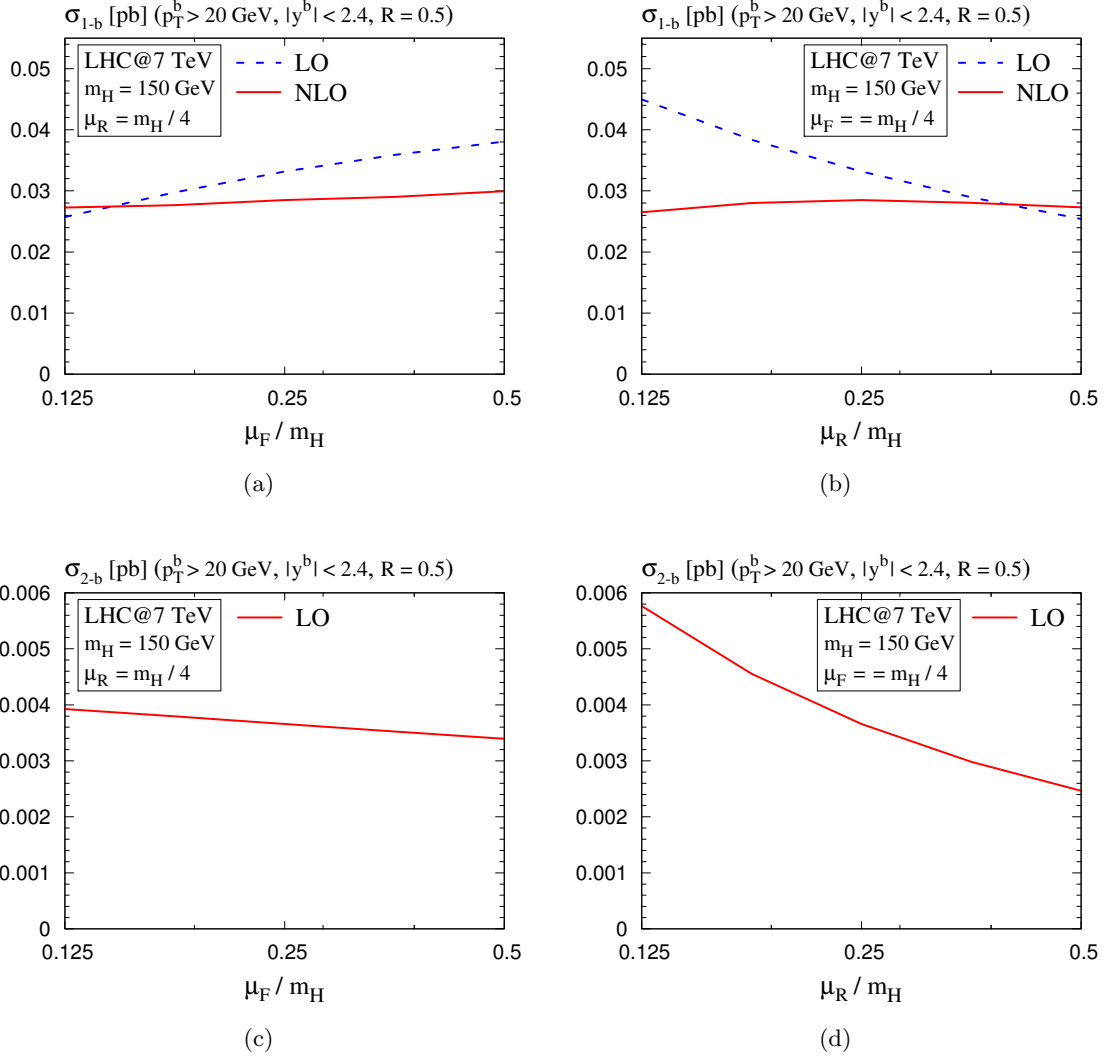


Figure 9: Scale dependence of (a),(b) the $H + 1b$ - and (c),(d) the $H + 2b$ -jet cross sections σ_{1b} and σ_{2b} ; (a),(c) μ_F -dependence, (b),(d) μ_R -dependence.

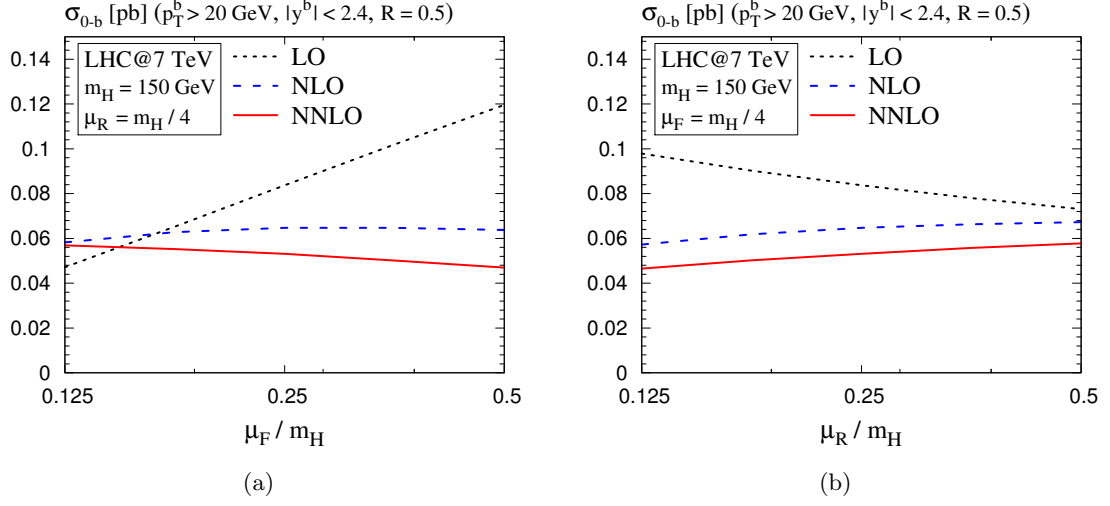


Figure 10: (a) μ_F - and (b) μ_R -dependence of the $H + 0b$ -jet cross section.

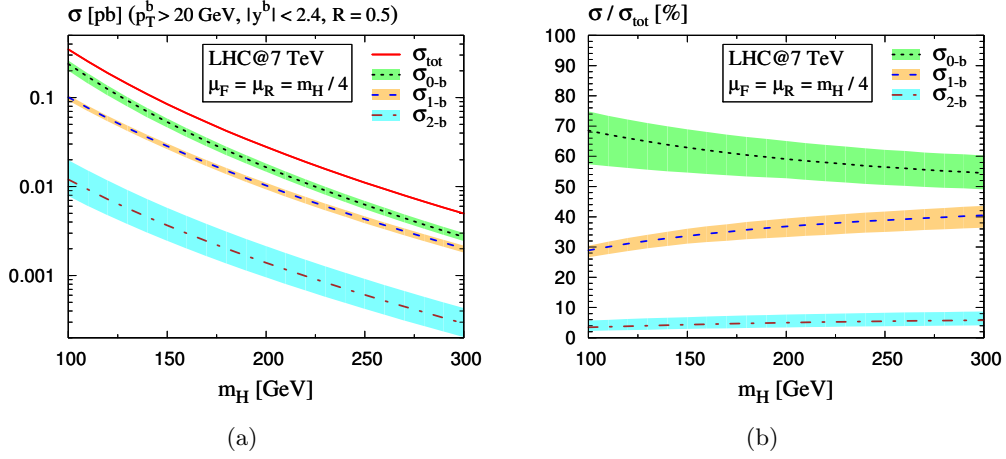


Figure 11: Higgs mass dependence of the $H + nb$ -jet contributions with respect to the total cross section (a) in absolute numbers and (b) relative to the total cross section.

The numerical results have been evaluated using realistic parameters for the LHC experiments and should be directly applicable to on-going analyses. Results for other parameters can be obtained from the authors upon request.

Acknowledgements. We would like to thank the Theory Group at CERN, where most of this work was done, for kind hospitality. We are indebted to Fabrice Couderc, Alexander Nikitenko, and Markus Schumacher for motivation and enlightening discussion, and to John Campbell for clarifications concerning MCFM. This work was supported by BMBF, contract 05H09PXE.

References

- [1] A. Djouadi, *The anatomy of electro-weak symmetry breaking. I: The Higgs boson in the standard model*, *Phys. Reports* **457** (2008) 1, [[hep-ph/0503172](#)].
- [2] A. Djouadi, *The anatomy of electro-weak symmetry breaking. II: The Higgs bosons in the minimal supersymmetric model*, *Phys. Reports* **459** (2008) 1, [[hep-ph/0503173](#)].
- [3] A. Belyaev, A. Blum, R.S. Chivukula, E.H. Simmons, *The meaning of Higgs: $\tau^+\tau^-$ and $\gamma\gamma$ at the Tevatron and the LHC*, *Phys. Rev. D* **72** (2005) 055022, [[hep-ph/0506086](#)].
- [4] S. Dittmaier, M. Krämer, M. Spira, *Higgs radiation off bottom quarks at the Tevatron and the LHC*, *Phys. Rev. D* **70** (2004) 074010, [[hep-ph/0309204](#)].
- [5] S. Dawson, C.B. Jackson, L. Reina, D. Wackeroth, *Exclusive Higgs boson production with bottom quarks at hadron colliders*, *Phys. Rev. D* **69** (2004) 074027, [[hep-ph/0311067](#)].
- [6] G. Gao, R.J. Oakes, J.M. Yang, *Heavy supersymmetric particle effects in Higgs boson production associated with a bottom quark pair at LHC*, *Phys. Rev. D* **71** (2005) 095005, [[hep-ph/0412356](#)].
- [7] R.V. Harlander and W.B. Kilgore, *Higgs boson production in bottom quark fusion at next-to-next-to-leading order*, *Phys. Rev. D* **68** (2003) 013001, [[hep-ph/0304035](#)].
- [8] S. Dittmaier, M. Krämer, A. Mück, T. Schlüter, *MSSM Higgs-boson production in bottom-quark fusion: Electroweak radiative corrections*, *JHEP* **0703** (2007) 114, [[hep-ph/0611353](#)].
- [9] D. Rainwater, M. Spira, D. Zeppenfeld, *Higgs boson production at hadron colliders: Signal and background processes*, [[hep-ph/0203187](#)].

- [10] T. Plehn, *Charged Higgs boson production in bottom-gluon fusion*, *Phys. Rev. D* **67** (2003) 014018, [[hep-ph/0206121](#)].
- [11] D. Dicus, T. Stelzer, Z. Sullivan, S. Willenbrock, *Higgs boson production in association with bottom quarks at next-to-leading order*, *Phys. Rev. D* **59** (1999) 094016, [[hep-ph/9811492](#)].
- [12] S. Dittmaier *et al.* [LHC Higgs Cross Section Working Group Collaboration], *Handbook of LHC Higgs Cross Sections: 1. Inclusive Observables*, [[arXiv:1101.0593](#)].
- [13] R. Harlander, M. Krämer, M. Schumacher, *Bottom-quark associated Higgs-boson production: reconciling the four- and five-flavour scheme approach*, LHC Higgs Cross Section Working Group Wiki Page, CERN-PH-TH/2011-134.
- [14] D. de Florian, M. Grazzini, Z. Kunszt, *Higgs production with large transverse momentum in hadronic collisions at next-to-leading order*, *Phys. Rev. Lett.* **82** (1999) 5209, [[hep-ph/9902483](#)].
- [15] C.J. Glosser and C.R. Schmidt, *Next-to-leading corrections to the Higgs boson transverse momentum spectrum in gluon fusion*, *JHEP* **0212** (2002) 016, [[hep-ph/0209248](#)].
- [16] V. Ravindran, J. Smith, W.L. van Neerven, *Next-to-leading order QCD corrections to differential distributions of Higgs boson production in hadron hadron collisions*, *Nucl. Phys. B* **634** (2002) 247, [[hep-ph/0201114](#)].
- [17] D. de Florian, M. Grazzini, *Next-to-next-to-leading logarithmic corrections at small transverse momentum in hadronic collisions*, *Phys. Rev. Lett.* **85** (2000) 4678, [[hep-ph/0008152](#)].
- [18] S. Catani, D. de Florian, M. Grazzini, *Direct Higgs production and jet veto at the Tevatron and the LHC in NNLO QCD*, *JHEP* **0201** (2002) 015, [[hep-ph/0111164](#)].
- [19] E.L. Berger and J.W. Qiu, *Differential cross section for Higgs boson production including all-orders soft gluon resummation*, *Phys. Rev. D* **67** (2003) 034026, [[hep-ph/0210135](#)].
- [20] G. Bozzi, S. Catani, D. de Florian, M. Grazzini, *Transverse-momentum resummation and the spectrum of the Higgs boson at the LHC*, *Nucl. Phys. B* **737** (2006) 73, [[hep-ph/0508068](#)].
- [21] C. Anastasiou, K. Melnikov, F. Petriello, *Higgs boson production at hadron colliders: Differential cross sections through next-to-next-to-leading order*, *Phys. Rev. Lett.* **93** (2004) 262002, [[hep-ph/0409088](#)].

- [22] C. Anastasiou, K. Melnikov, F. Petriello, *Fully differential Higgs boson production and the di-photon signal through next-to-next-to-leading order*, *Nucl. Phys. B* **724** (2005) 197, [[hep-ph/0501130](#)].
- [23] J.M. Campbell, R.K. Ellis, G. Zanderighi, *Next-to-leading order Higgs + 2 jet production via gluon fusion*, *JHEP* **0610** (2006) 028, [[hep-ph/0608194](#)].
- [24] S. Catani and M. Grazzini, *An NNLO subtraction formalism in hadron collisions and its application to Higgs boson production at the LHC*, *Phys. Rev. Lett.* **98** (2007) 222002, [[hep-ph/0703012](#)].
- [25] G. Bozzi, S. Catani, D. de Florian, M. Grazzini, *Higgs boson production at the LHC: Transverse-momentum resummation and rapidity dependence*, *Nucl. Phys. B* **791** (2008) 1, [[arXiv:0705.3887](#)].
- [26] C.F. Berger, C. Marcantonini, I.W. Stewart, F.J. Tackmann, W.J. Waalewijn, *Higgs Production with a Central Jet Veto at NNLL+NNLO*, *JHEP* **1104** (2011) 092, [[arXiv:1012.4480](#)].
- [27] B. Field, J. Smith, M.E. Tejeda-Yeomans, W.L. van Neerven, *NLO corrections to differential cross sections for pseudo-scalar Higgs boson production*, *Phys. Lett. B* **551** (2003) 137, [[hep-ph/0210369](#)].
- [28] B. Field, S. Dawson, J. Smith, *Scalar and pseudoscalar Higgs boson plus one jet production at the LHC and Tevatron*, *Phys. Rev. D* **69** (2004) 074013, [[hep-ph/0311199](#)].
- [29] U. Langenegger, M. Spira, A. Starodumov, P. Trueb, *SM and MSSM Higgs Boson Production: Spectra at large transverse Momentum*, *JHEP* **0606** (2006) 035, [[hep-ph/0604156](#)].
- [30] O. Brein and W. Hollik, *MSSM Higgs bosons associated with high- p_T jets at hadron colliders*, *Phys. Rev. D* **68** (2003) 095006, [[hep-ph/0305321](#)].
- [31] O. Brein and W. Hollik, *Distributions for MSSM Higgs boson + jet production at hadron colliders*, *Phys. Rev. D* **76** (2007) 035002, [[arXiv:0705.2744](#)].
- [32] O. Brein, *Electroweak and Bottom Quark Contributions to Higgs Boson plus Jet Production*, *Phys. Rev. D* **81** (2010) 093006, [[arXiv:1003.4438](#)].
- [33] S. Dawson, C.B. Jackson, P. Jaiswal, *SUSY QCD Corrections to Higgs-b Production: Is the Δm_b Approximation Accurate?*, [[arXiv:1104.1631](#)].
- [34] R.V. Harlander, K.J. Ozeren, M. Wiesemann, *Higgs plus jet production in bottom quark annihilation at next-to-leading order*, *Phys. Lett. B* **693** (2010) 269, [[arXiv:1007.5411](#)].

- [35] J. Campbell, R.K. Ellis, F. Maltoni, S. Willenbrock, *Higgs boson production in association with a single bottom quark*, *Phys. Rev. D* **67** (2003) 095002, [[hep-ph/0204093](#)].
- [36] S. Dawson, C.B. Jackson, L. Reina, D. Wackerroth, *Higgs boson production with one bottom quark jet at hadron colliders*, *Phys. Rev. Lett.* **94** (2005) 031802, [[hep-ph/0408077](#)].
- [37] M. Cacciari, G.P. Salam, G. Soyez, *The anti- k_T jet clustering algorithm*, *JHEP* **0804** (2008) 063, [[arXiv:0802.1189](#)].
- [38] J. Campbell and R.K. Ellis, *MCFM*, <http://mcfm.fnal.gov>.
- [39] A.D. Martin, W.J. Stirling, R.S. Thorne, G. Watt, *Parton distributions for the LHC*, *Eur. Phys. J. C* **63** (2009) 189, [[arXiv:0901.0002](#)].
- [40] C. Anastasiou, G. Dissertori, M. Grazzini, F. Stöckli, B.R. Webber, *Perturbative QCD effects and the search for a $H \rightarrow WW \rightarrow l\nu l\nu$ signal at the Tevatron*, *JHEP* **0908** (2009) 099, [[arXiv:0905.3529](#)].
- [41] I.W. Stewart, F.J. Tackmann, *Theory Uncertainties for Higgs and Other Searches Using Jet Bins*, [[arXiv:1107.2117](#)].

A Numerical values for the LHC at 7 TeV

LHC @ 7 TeV, $ y^{\text{jet}} < 4.8$, $p_T^{\text{jet}} > 20 \text{ GeV}$, $R = 0.4$						
m_H [GeV]	$\sigma_{0\text{-jet}}^{\text{NNLO}}$ [fb]	scale [%]	PDF [%]	$\sigma_{\geq 1\text{-jet}}^{\text{NLO}}$ [fb]	scale [%]	PDF [%]
100	184	+14.0 -20.9	+5.1 -4.1	167	+3.5 -9.9	+3.0 -6.7
110	128	+14.1 -20.0	+5.3 -4.0	126	+3.3 -9.0	+3.5 -6.2
120	92.0	+14.3 -19.0	+5.4 -3.8	97.5	+3.1 -8.2	+4.0 -5.6
130	67.0	+14.4 -18.1	+5.5 -3.7	75.9	+3.0 -7.4	+4.5 -5.0
140	49.4	+14.6 -17.1	+5.7 -3.6	59.7	+2.8 -6.5	+5.0 -4.4
150	37.1	+14.7 -16.2	+5.8 -3.4	47.4	+2.6 -5.7	+5.5 -3.9
160	28.2	+14.6 -16.1	+5.7 -3.8	38.3	+2.6 -5.7	+5.6 -3.8
170	21.6	+14.5 -16.0	+5.6 -4.2	31.0	+2.6 -5.7	+5.6 -3.8
180	16.8	+14.4 -15.9	+5.4 -4.6	25.4	+2.5 -5.6	+5.7 -3.8
190	13.3	+14.3 -15.9	+5.3 -4.9	20.9	+2.5 -5.6	+5.7 -3.7
200	10.5	+14.2 -15.8	+5.2 -5.3	17.3	+2.5 -5.6	+5.8 -3.7
210	8.43	+14.1 -15.5	+5.2 -5.7	14.4	+2.5 -6.1	+6.1 -3.8
220	6.75	+14.0 -15.2	+5.2 -6.1	12.1	+2.5 -6.5	+6.4 -4.0
230	5.49	+13.9 -14.9	+5.3 -6.4	10.2	+2.5 -7.0	+6.8 -4.2
240	4.49	+13.8 -14.6	+5.3 -6.8	8.64	+2.5 -7.4	+7.1 -4.3
250	3.71	+13.7 -14.2	+5.3 -7.2	7.36	+2.5 -7.9	+7.4 -4.5
260	3.04	+13.6 -14.4	+6.1 -6.7	6.28	+2.5 -8.1	+6.9 -5.3
270	2.49	+13.4 -14.5	+6.8 -6.2	5.38	+2.6 -8.3	+6.3 -6.0
280	2.11	+13.3 -14.7	+7.6 -5.8	4.64	+2.7 -8.5	+5.8 -6.8
290	1.77	+13.2 -14.8	+8.4 -5.3	4.01	+2.8 -8.6	+5.2 -7.6
300	1.50	+13.1 -14.9	+9.1 -4.8	3.47	+2.8 -8.8	+4.7 -8.4

Table 1: Central values, scale and PDF uncertainties for the exclusive $H + 0\text{-jet}$ (NNLO) and inclusive $H + \text{jet}$ (NLO) cross section for $|y^{\text{jet}}| < 4.8$, see also Fig. 6 (a).

LHC @ 7 TeV, $ y^{\text{jet}} < 2.5$, $p_T^{\text{jet}} > 20$ GeV, $R = 0.4$						
m_H [GeV]	$\sigma_{0\text{-jet}}^{\text{NNLO}}$ [fb]	scale [%]	PDF [%]	$\sigma_{\geq 1\text{-jet}}^{\text{NLO}}$ [fb]	scale [%]	PDF [%]
100	209	+10.9 -17.7	+3.2 -3.1	141	+3.6 -9.2	+3.7 -4.6
110	146	+10.9 -16.8	+3.5 -3.0	107	+3.0 -8.4	+4.0 -4.4
120	106	+10.9 -15.9	+3.8 -2.9	82.5	+2.4 -7.6	+4.2 -4.2
130	77.4	+10.9 -14.9	+4.1 -2.9	64.5	+1.8 -6.8	+4.5 -4.0
140	57.9	+10.9 -14.0	+4.4 -2.8	50.9	+1.2 -6.0	+4.7 -3.8
150	44.0	+10.9 -13.1	+4.7 -2.7	40.7	+0.5 -5.2	+5.0 -3.6
160	33.5	+10.8 -12.7	+4.5 -3.3	32.6	+0.8 -5.6	+5.2 -3.6
170	26.2	+10.7 -12.3	+4.3 -3.9	26.6	+1.0 -6.0	+5.4 -3.7
180	20.4	+10.6 -11.9	+4.1 -4.6	21.8	+1.2 -6.4	+5.6 -3.8
190	16.1	+10.5 -11.5	+3.9 -5.2	17.9	+1.5 -6.7	+5.8 -3.9
200	12.9	+10.4 -11.1	+3.6 -5.8	14.9	+1.7 -7.1	+6.1 -3.9
210	10.4	+10.2 -11.0	+4.2 -5.8	12.4	+1.7 -7.5	+5.9 -4.1
220	8.34	+10.0 -10.9	+4.8 -5.7	10.4	+1.7 -7.8	+5.6 -4.3
230	6.84	+9.8 -10.8	+5.4 -5.7	8.81	+1.8 -8.1	+5.4 -4.5
240	5.68	+9.6 -10.7	+6.0 -5.6	7.49	+1.8 -8.4	+5.2 -4.7
250	4.66	+9.3 -10.6	+6.6 -5.6	6.37	+1.8 -8.7	+5.0 -4.9
260	3.87	+9.3 -10.5	+6.4 -6.1	5.44	+2.0 -9.0	+5.1 -5.2
270	3.25	+9.3 -10.5	+6.1 -6.7	4.67	+2.1 -9.2	+5.2 -5.5
280	2.72	+9.3 -10.4	+5.9 -7.2	4.01	+2.3 -9.5	+5.2 -5.8
290	2.32	+9.2 -10.4	+5.7 -7.7	3.48	+2.5 -9.7	+5.3 -6.1
300	1.93	+9.2 -10.3	+5.4 -8.3	3.02	+2.6 -10.0	+5.4 -6.4

Table 2: Same as Table 1, but for $|y^{\text{jet}}| < 2.5$, see also Fig. 6 (b).

LHC @ 7 TeV						
m_H [GeV]	$\sigma_{\text{tot}}^{\text{NNLO}}$ [fb]	scale [%]	$p_T^{\text{jet}} > 20 \text{ GeV}, R = 0.4$			
			$ y^{\text{jet}} < 4.8$		$ y^{\text{jet}} < 2.5$	
			$\sigma_{\geq 1\text{-jet}}^{\text{NLO}'}$ [fb]	scale [%]	$\sigma_{\geq 1\text{-jet}}^{\text{NLO}'}$ [fb]	scale [%]
100	349	+2.9 -10.0	165	+2.1 -9.4	140	+3.4 -9.0
110	254	+3.0 -9.6	126	+2.1 -8.6	108	+3.0 -8.2
120	188	+3.1 -9.1	96.3	+2.0 -7.9	82.4	+2.7 -7.4
130	142	+3.1 -8.7	75.1	+2.0 -7.2	64.7	+2.3 -6.6
140	109	+3.2 -8.3	59.4	+1.9 -6.4	50.9	+1.9 -5.8
150	84.5	+3.2 -7.8	47.4	+1.9 -5.7	40.5	+1.5 -5.1
160	66.4	+3.2 -7.6	38.2	+1.7 -5.5	32.9	+1.6 -5.3
170	52.7	+3.2 -7.5	31.1	+1.6 -5.3	26.5	+1.6 -5.5
180	42.3	+3.2 -7.3	25.4	+1.4 -5.1	21.9	+1.6 -5.7
190	34.2	+3.2 -7.1	20.9	+1.3 -4.9	18.1	+1.7 -6.0
200	27.9	+3.2 -6.9	17.4	+1.1 -4.8	15.0	+1.7 -6.2
210	22.9	+3.2 -6.8	14.5	+1.4 -5.2	12.5	+1.8 -6.4
220	18.9	+3.2 -6.7	12.2	+1.7 -5.7	10.6	+1.9 -6.7
230	15.7	+3.1 -6.5	10.2	+1.9 -6.1	8.90	+2.1 -6.9
240	13.2	+3.1 -6.4	8.68	+2.2 -6.6	7.49	+2.2 -7.2
250	11.1	+3.1 -6.3	7.37	+2.4 -7.1	6.42	+2.3 -7.4
260	9.36	+3.1 -6.2	6.31	+2.5 -7.3	5.49	+2.3 -7.7
270	7.95	+3.1 -6.1	5.46	+2.6 -7.6	4.70	+2.4 -8.0
280	6.78	+3.0 -5.9	4.67	+2.7 -7.8	4.05	+2.4 -8.4
290	5.80	+3.0 -5.8	4.03	+2.8 -8.1	3.48	+2.5 -8.7
300	4.98	+3.0 -5.7	3.48	+2.9 -8.3	3.06	+2.5 -9.0

Table 3: Total cross section $\sigma_{\text{tot}}^{\text{NNLO}}$, and $\sigma_{\geq 1\text{-jet}}^{\text{NLO}'}$ for two different jet rapidity cuts, including the associated scale uncertainties.

LHC @ 7 TeV, $ y^b < 2.4$, $p_T^b > 20$ GeV, $R = 0.5$									
m_H [GeV]	$\sigma_{0b}^{\text{NNLO}}$ [fb]	scale [%]	PDF [%]	σ_{1b}^{NLO} [fb]	scale [%]	PDF [%]	σ_{2b}^{LO} [fb]	scale [%]	PDF [%]
100	239	+8.3 -15.9	+3.8 -3.2	101	+4.1 -7.0	+3.4 -3.8	12.0	+64.7 -34.8	+2.5 -2.6
110	170	+8.5 -15.2	+3.8 -3.5	76.3	+4.2 -7.0	+3.8 -3.6	9.24	+63.3 -34.4	+2.4 -2.7
120	124	+8.6 -14.4	+3.7 -3.9	58.6	+4.3 -7.0	+4.2 -3.5	7.20	+61.9 -34.0	+2.4 -2.8
130	92.2	+8.7 -13.7	+3.7 -4.2	45.5	+4.3 -6.9	+4.6 -3.4	5.69	+60.5 -33.5	+2.4 -2.9
140	69.5	+8.8 -12.9	+3.6 -4.6	35.8	+4.4 -6.9	+5.0 -3.2	4.54	+59.0 -33.1	+2.3 -3.0
150	53.1	+9.0 -12.2	+3.6 -4.9	28.4	+4.5 -6.9	+5.4 -3.1	3.66	+57.6 -32.7	+2.3 -3.1
160	41.2	+9.0 -11.7	+3.7 -4.8	22.9	+4.7 -7.2	+5.4 -3.4	2.97	+56.8 -32.4	+2.4 -3.1
170	32.3	+9.0 -11.3	+3.9 -4.6	18.5	+4.8 -7.5	+5.3 -3.6	2.44	+56.0 -32.1	+2.4 -3.1
180	25.6	+9.1 -10.8	+4.0 -4.5	15.1	+4.9 -7.9	+5.2 -3.9	2.01	+55.2 -31.8	+2.5 -3.1
190	20.5	+9.1 -10.4	+4.1 -4.4	12.4	+5.0 -8.2	+5.1 -4.1	1.67	+54.3 -31.6	+2.6 -3.2
200	16.5	+9.1 -9.9	+4.3 -4.2	10.3	+5.1 -8.5	+5.1 -4.4	1.39	+53.5 -31.3	+2.6 -3.2
210	13.4	+9.1 -9.8	+4.3 -4.3	8.53	+5.2 -8.5	+5.0 -4.5	1.17	+52.9 -31.1	+2.8 -3.2
220	11.0	+9.1 -9.7	+4.4 -4.4	7.13	+5.3 -8.5	+5.0 -4.6	0.985	+52.4 -30.9	+2.9 -3.2
230	9.04	+9.0 -9.6	+4.5 -4.5	6.01	+5.3 -8.6	+5.0 -4.7	0.835	+51.8 -30.7	+3.1 -3.2
240	7.49	+9.0 -9.5	+4.6 -4.6	5.08	+5.4 -8.6	+4.9 -4.9	0.710	+51.3 -30.5	+3.2 -3.2
250	6.25	+9.0 -9.4	+4.7 -4.7	4.30	+5.4 -8.6	+4.9 -5.0	0.607	+50.7 -30.3	+3.4 -3.2
260	5.24	+9.0 -9.2	+4.9 -4.9	3.67	+5.5 -8.7	+5.0 -4.9	0.520	+50.3 -30.1	+3.4 -3.3
270	4.41	+9.0 -8.9	+5.1 -5.0	3.14	+5.5 -8.7	+5.0 -4.9	0.448	+49.8 -30.0	+3.4 -3.4
280	3.74	+9.0 -8.7	+5.3 -5.1	2.70	+5.6 -8.7	+5.1 -4.8	0.386	+49.4 -29.8	+3.5 -3.4
290	3.18	+8.9 -8.5	+5.5 -5.3	2.33	+5.6 -8.8	+5.2 -4.8	0.335	+49.0 -29.7	+3.5 -3.5
300	2.71	+8.9 -8.2	+5.7 -5.4	2.02	+5.7 -8.8	+5.3 -4.7	0.291	+48.6 -29.5	+3.5 -3.5

Table 4: Central values, scale and PDF uncertainties for the exclusive $H + nb$ -jet ($n = 0, 1, 2$) cross section at NNLO, NLO, and LO, respectively. See also Fig. 11.

B Results for the LHC at 14 TeV

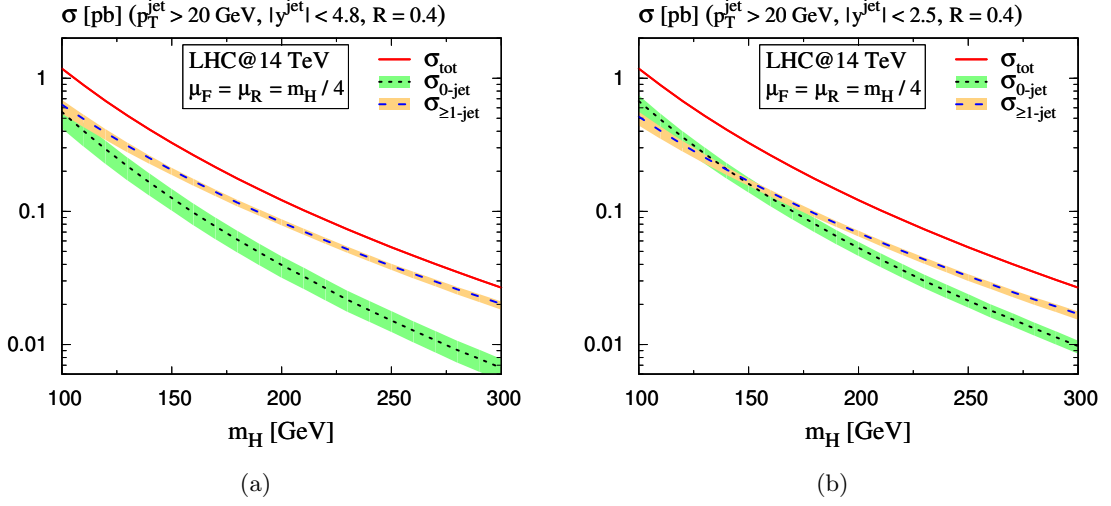


Figure 12: Higgs mass dependence of the $H + 0$ - and ≥ 1 -jet contributions to the total cross section at NNLO and NLO, respectively, for (a) $|y^{\text{jet}}| < 4.8$ and (b) $|y^{\text{jet}}| < 2.5$.

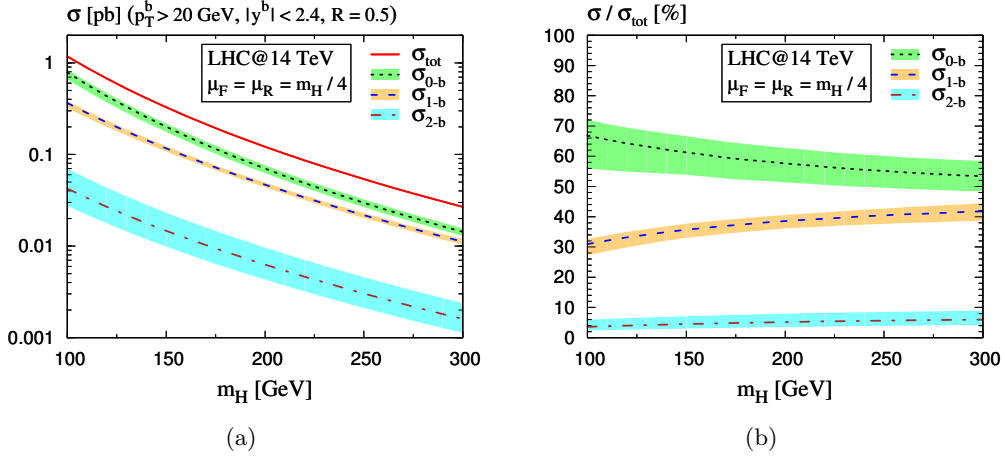


Figure 13: Higgs mass dependence of the $H + nb$ -jet contributions with respect to the total cross section (a) in absolute numbers and (b) relative to the total cross section.

LHC @ 14 TeV, $ y^{\text{jet}} < 4.8$, $p_T^{\text{jet}} > 20 \text{ GeV}$, $R = 0.4$						
m_H [GeV]	$\sigma_{0\text{-jet}}^{\text{NNLO}}$ [fb]	scale [%]	PDF [%]	$\sigma_{\geq 1\text{-jet}}^{\text{NLO}}$ [fb]	scale [%]	PDF [%]
100	558	+14.4 -24.6	+3.2 -3.1	632	+8.3 -13.3	+2.6 -4.6
110	400	+14.9 -23.4	+3.3 -3.7	492	+7.2 -12.2	+2.7 -4.3
120	292	+15.4 -22.3	+3.3 -4.2	388	+6.0 -11.1	+2.7 -4.0
130	217	+15.9 -21.1	+3.4 -4.7	310	+4.9 -9.9	+2.7 -3.7
140	165	+16.3 -19.9	+3.5 -5.2	251	+3.8 -8.8	+2.7 -3.4
150	126	+16.8 -18.8	+3.5 -5.7	204	+2.6 -7.6	+2.8 -3.1
160	97.7	+16.6 -18.7	+3.2 -6.1	168	+2.4 -7.0	+3.3 -3.0
170	76.8	+16.5 -18.6	+2.8 -6.6	139	+2.3 -6.4	+3.8 -2.8
180	61.2	+16.3 -18.6	+2.5 -7.0	116	+2.1 -5.7	+4.2 -2.7
190	49.0	+16.1 -18.5	+2.2 -7.4	98.0	+1.9 -5.1	+4.7 -2.5
200	39.6	+15.9 -18.4	+1.8 -7.8	82.7	+1.7 -4.4	+5.2 -2.4
210	32.5	+15.9 -18.0	+2.9 -7.6	70.7	+1.6 -4.8	+4.9 -2.5
220	26.5	+16.0 -17.6	+3.9 -7.5	60.4	+1.5 -5.1	+4.6 -2.6
230	21.7	+16.0 -17.2	+5.0 -7.3	52.0	+1.3 -5.4	+4.3 -2.7
240	18.1	+16.1 -16.8	+6.1 -7.1	44.9	+1.2 -5.8	+4.0 -2.8
250	15.1	+16.1 -16.4	+7.1 -6.9	39.0	+1.1 -6.1	+3.6 -2.9
260	12.7	+16.0 -16.8	+7.1 -7.6	33.9	+1.4 -6.5	+3.6 -3.3
270	10.8	+15.8 -17.1	+7.0 -8.2	29.7	+1.6 -6.9	+3.6 -3.8
280	9.09	+15.7 -17.4	+7.0 -8.9	26.0	+1.9 -7.3	+3.6 -4.2
290	7.83	+15.5 -17.7	+6.9 -9.5	22.9	+2.2 -7.7	+3.6 -4.6
300	6.68	+15.4 -18.0	+6.8 -10.2	20.2	+2.5 -8.1	+3.5 -5.1

Table 5: Central values, scale and PDF uncertainties for the exclusive $H + 0\text{-jet}$ (NNLO) and inclusive $H + \text{jet}$ (NLO) cross section for $|y^{\text{jet}}| < 2.5$, see also Fig. 12 (a).

LHC @ 14 TeV, $ y^{\text{jet}} < 2.5$, $p_T^{\text{jet}} > 20 \text{ GeV}$, $R = 0.4$						
m_H [GeV]	$\sigma_{0\text{-jet}}^{\text{NNLO}}$ [fb]	scale [%]	PDF [%]	$\sigma_{\geq 1\text{-jet}}^{\text{NLO}}$ [fb]	scale [%]	PDF [%]
100	673	+10.2 -18.8	+2.7 -3.7	514	+8.4 -13.5	+3.1 -4.3
110	487	+10.4 -17.8	+2.9 -3.3	401	+7.1 -12.2	+3.3 -4.0
120	360	+10.5 -16.8	+3.1 -3.0	317	+5.7 -10.8	+3.4 -3.7
130	271	+10.7 -15.8	+3.3 -2.6	254	+4.3 -9.5	+3.6 -3.4
140	207	+10.9 -14.8	+3.5 -2.2	206	+3.0 -8.2	+3.8 -3.1
150	161	+11.1 -13.9	+3.7 -1.8	168	+1.6 -6.9	+3.9 -2.7
160	126	+11.0 -13.4	+3.7 -2.6	139	+1.5 -6.6	+3.9 -2.7
170	100	+10.8 -12.9	+3.6 -3.4	115	+1.4 -6.2	+3.9 -2.7
180	80.5	+10.7 -12.4	+3.5 -4.2	96.6	+1.4 -5.9	+3.9 -2.7
190	65.0	+10.6 -12.0	+3.5 -5.1	81.3	+1.3 -5.6	+3.8 -2.7
200	53.2	+10.4 -11.5	+3.4 -5.9	68.9	+1.2 -5.3	+3.8 -2.6
210	43.7	+10.5 -11.3	+3.7 -5.5	58.6	+1.3 -5.4	+3.7 -3.1
220	36.2	+10.5 -11.1	+3.9 -5.1	50.4	+1.4 -5.5	+3.5 -3.6
230	30.1	+10.5 -10.9	+4.2 -4.7	43.5	+1.5 -5.7	+3.4 -4.0
240	25.3	+10.6 -10.8	+4.5 -4.3	37.6	+1.6 -5.8	+3.2 -4.5
250	21.4	+10.6 -10.6	+4.7 -3.9	32.6	+1.7 -5.9	+3.1 -5.0
260	18.1	+10.3 -10.4	+4.8 -4.7	28.5	+1.7 -6.3	+3.2 -5.0
270	15.5	+9.9 -10.1	+4.9 -5.4	24.8	+1.8 -6.7	+3.4 -5.1
280	13.2	+9.5 -9.9	+5.0 -6.2	21.8	+1.9 -7.0	+3.5 -5.2
290	11.4	+9.2 -9.7	+5.0 -6.9	19.3	+2.0 -7.4	+3.7 -5.2
300	9.73	+8.8 -9.5	+5.1 -7.7	17.0	+2.1 -7.8	+3.8 -5.3

Table 6: Same as Table 5, but for $|y^{\text{jet}}| < 2.5$, see also Fig. 12 (b).

LHC @ 14 TeV						
m_H [GeV]	$\sigma_{\text{tot}}^{\text{NNLO}}$ [fb]	scale [%]	$p_T^{\text{jet}} > 20 \text{ GeV}, R = 0.4$			
			$ y^{\text{jet}} < 4.8$		$ y^{\text{jet}} < 2.5$	
			$\sigma_{\geq 1\text{-jet}}^{\text{NLO}'}$ [fb]	scale [%]	$\sigma_{\geq 1\text{-jet}}^{\text{NLO}'}$ [fb]	scale [%]
100	1178	+1.2 -9.5	620	+8.2 -12.7	505	+8.6 -12.1
110	882	+1.3 -8.8	482	+6.9 -11.7	395	+7.1 -11.1
120	673	+1.4 -8.1	381	+5.6 -10.6	313	+5.5 -10.1
130	522	+1.5 -7.4	305	+4.3 -9.6	251	+4.0 -9.1
140	411	+1.7 -6.7	246	+3.0 -8.5	203	+2.4 -8.1
150	327	+1.8 -6.0	201	+1.7 -7.5	166	+0.9 -7.1
160	263	+1.8 -5.9	166	+1.8 -6.9	137	+0.9 -6.6
170	214	+1.9 -5.8	137	+1.9 -6.3	114	+0.9 -6.1
180	176	+2.0 -5.8	115	+2.0 -5.8	95.5	+0.9 -5.5
190	146	+2.0 -5.7	96.7	+2.1 -5.2	80.7	+0.9 -5.0
200	121	+2.1 -5.6	81.9	+2.2 -4.6	68.3	+0.9 -4.5
210	102	+2.1 -5.5	69.5	+2.1 -4.8	58.3	+1.0 -4.7
220	86.2	+2.1 -5.5	59.7	+1.9 -5.1	50.1	+1.0 -5.0
230	73.3	+2.1 -5.4	51.6	+1.8 -5.3	43.2	+1.0 -5.2
240	62.7	+2.1 -5.3	44.6	+1.7 -5.5	37.4	+1.1 -5.4
250	53.8	+2.1 -5.3	38.7	+1.5 -5.7	32.4	+1.1 -5.7
260	46.4	+2.1 -5.2	33.7	+1.6 -6.1	28.3	+1.1 -5.9
270	40.2	+2.1 -5.1	29.5	+1.8 -6.5	24.7	+1.0 -6.1
280	35.0	+2.1 -5.1	25.9	+1.9 -6.8	21.8	+1.0 -6.2
290	30.6	+2.1 -5.0	22.7	+2.0 -7.2	19.2	+1.0 -6.4
300	26.8	+2.1 -4.9	20.1	+2.1 -7.6	17.1	+0.9 -6.6

Table 7: Total cross section $\sigma_{\text{tot}}^{\text{NNLO}}$, and $\sigma_{\geq 1\text{-jet}}^{\text{NLO}'}$ for two different jet rapidity cuts, including the associated scale uncertainties.

LHC @ 14 TeV, $ y^b < 2.4$, $p_T^b > 20$ GeV, $R = 0.5$									
m_H [GeV]	$\sigma_{0b}^{\text{NNLO}}$ [fb]	scale [%]	PDF [%]	σ_{1b}^{NLO} [fb]	scale [%]	PDF [%]	σ_{2b}^{LO} [fb]	scale [%]	PDF [%]
100	787	+7.1 -16.0	+3.0 -2.4	364	+4.4 -11.4	+3.2 -2.7	42.3	+64.7 -34.8	+1.8 -2.5
110	577	+7.3 -15.2	+3.0 -2.6	283	+4.3 -10.4	+3.4 -2.9	33.4	+63.3 -34.4	+1.8 -2.5
120	432	+7.6 -14.3	+2.9 -2.8	223	+4.1 -9.5	+3.6 -3.1	26.8	+61.8 -34.0	+1.7 -2.6
130	330	+7.8 -13.4	+2.9 -2.9	178	+4.0 -8.5	+3.8 -3.2	21.7	+60.4 -33.6	+1.7 -2.6
140	255	+8.1 -12.5	+2.8 -3.1	143	+3.9 -7.6	+3.9 -3.4	17.8	+59.0 -33.1	+1.7 -2.7
150	200	+8.3 -11.6	+2.7 -3.3	117	+3.7 -6.6	+4.1 -3.5	14.7	+57.6 -32.7	+1.7 -2.7
160	159	+8.3 -11.4	+2.8 -3.2	95.7	+3.7 -6.3	+4.0 -3.6	12.2	+56.8 -32.4	+1.8 -2.7
170	128	+8.3 -11.2	+2.9 -3.0	79.2	+3.7 -5.9	+3.9 -3.7	10.3	+55.9 -32.1	+1.9 -2.6
180	104	+8.3 -11.0	+3.0 -2.9	66.0	+3.8 -5.6	+3.8 -3.8	8.66	+55.1 -31.9	+2.0 -2.6
190	84.9	+8.3 -10.8	+3.1 -2.7	55.5	+3.8 -5.2	+3.7 -3.9	7.35	+54.2 -31.6	+2.0 -2.5
200	70.0	+8.3 -10.6	+3.1 -2.6	46.8	+3.8 -4.9	+3.6 -4.0	6.27	+53.4 -31.3	+2.1 -2.5
210	58.3	+8.3 -10.3	+3.2 -2.8	39.8	+3.8 -5.1	+3.7 -4.0	5.38	+52.8 -31.1	+2.1 -2.5
220	48.7	+8.3 -10.1	+3.2 -3.0	33.9	+3.9 -5.2	+3.7 -3.9	4.64	+52.3 -30.9	+2.1 -2.5
230	41.0	+8.4 -9.9	+3.3 -3.3	29.1	+3.9 -5.4	+3.8 -3.9	4.01	+51.7 -30.7	+2.1 -2.6
240	34.8	+8.4 -9.7	+3.3 -3.5	25.1	+4.0 -5.6	+3.8 -3.9	3.48	+51.2 -30.5	+2.1 -2.6
250	29.7	+8.4 -9.4	+3.3 -3.7	21.8	+4.0 -5.7	+3.9 -3.8	3.04	+50.6 -30.4	+2.1 -2.6
260	25.4	+8.4 -9.2	+3.4 -3.8	18.9	+4.1 -5.9	+4.0 -3.8	2.66	+50.2 -30.2	+2.2 -2.7
270	21.9	+8.5 -9.0	+3.6 -3.9	16.5	+4.1 -6.1	+4.2 -3.7	2.33	+49.8 -30.0	+2.2 -2.7
280	18.9	+8.5 -8.8	+3.7 -4.0	14.4	+4.2 -6.2	+4.4 -3.7	2.05	+49.3 -29.9	+2.3 -2.7
290	16.4	+8.5 -8.6	+3.8 -4.1	12.7	+4.3 -6.4	+4.6 -3.6	1.81	+48.9 -29.7	+2.3 -2.7
300	14.3	+8.6 -8.4	+3.9 -4.2	11.2	+4.4 -6.6	+4.7 -3.5	1.60	+48.5 -29.6	+2.4 -2.8

Table 8: Central values, scale and PDF uncertainties for the exclusive $H + nb$ -jet ($n = 0, 1, 2$) cross section at NNLO, NLO, and LO, respectively. See also Fig. 13.